Development of Laser Systems and Spectroscopy of Highly Charged Ions

Zur Erlangung des Grades eines Doktors der Naturwissenschaften (Dr. rer. nat.)
Vorgelegte Dissertation von Patrick Baus aus Mannheim
Tag der Einreichung: 1. November 2022, Tag der Prüfung: 1. November 2022

1. Gutachten: Prof. Dr. Gerhard Birkl
Foobar

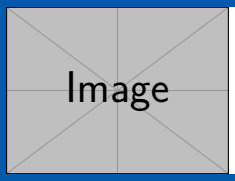

Physics Department
Institut für Angewandte Physik
APQ

Development of Laser Systems and Spectroscopy of Highly Charged Ions

Submitted doctoral thesis by Patrick Baus

1. Review: Prof. Dr. Gerhard Birkl

Date of submission: November 1, 2022
Date of thesis defense: November 1, 2022

Foobar

1. Preparation

1.1. Grounding and Shielding

Add parts from ”references
Grounding and Shielding.pdf”

1.2. Laser Current Driver

1.2.1. Design

Simulation

Op Amp Stability

1.2.2. Noise Considerations

1.2.3. Voltage Reference

1.2.4. MOSFET Selection

1.3. LabKraken

1.3.1. Design Goals

LabKraken is a designed to be a asynchronous, resilient data aquisition suite, that scales to thousands of sensors and accross different networks.

1.3.2. Hardware

1.3.3. Software Architecture

LabKraken needs to scale to thousands of sensors, which need to be served concurrently. This problem is commonly referered to as the C10K problem as dubbed by Dan Kegel back in 1999 [21] and refers to serving 10 000 concurrent connections via network sockets. While today millions of concurrent connections can be handled by servers, handling 10 000 can still be challenging, especially, if the data sources are heterogeneous as is typical for sensor networks of different sensors from different manufacturers.

In order to meet the design goals, an asynchronous architecture was chosen and several different architectures were implemented over time. All in all four complete rewrites of the software were made to arrive at the architecture presented here. The reason for the rewrites is mostly historic and can be explained by the history of the programming language Python, which was used to write the code. The first first version was written for Python 2.6 and

exclusively supported sensors made Tinkerforge. In 2015, Python 3.5 was released, which supported a new syntax for asynchronous coroutines. The software was rewritten from scratch to support this new syntax, because it made the code a lot more verbose and easier to follow. With the release of Python 3.7 in 2018 asynchronous generator expressions where mature enough to be used in productions and the programm was again rewritten to use the new syntax. In 2021 a new approach was taken and the programm was once more rewritten with a functional programming style. I will discuss each approach in the next sections to highlight the improvements, that were made over time. Each of these sections discusses the same programm, but written in different styles to show the differences.

Threaded Design

The first version of LabKraken used a threaded design approach, because the original libraries of the Tinkerforge sensors are built around threads. The following simplified example shows some code to connect to a temperature sensor over the network and read its data.

```
ipcon = IPConnection()
devices = dict()

# Callback function for temperature callback
def cb_temperature(temperature):
    print("Temperature: " + str(temperature/100.0) + " degC")

def cb_connected(connect_reason)::
    ipcon.enumerate()

def cb_disconnected(disconnect_reason)::
    log_reason(disconnect_reason)

def cb_enumerate(uid, *_args):
    if uid == OUR_KNOWN_DEVICE:
        dev = BrickletTemperatureV2(uid, ipcon)
        # Register temperature callback to function cb_temperature
        dev.register_callback(dev.CALLBACK_TEMPERATURE, cb_temperature)
        dev.set_temperature_callback_configuration(1000, False, "x", 0, 0)
        devives[uid] = dev

if __name__ == "__main__":
    ipcon.connect(HOST, PORT)  # blocking call
    # Register Enumerate Callback
    ipcon.register_callback(IPConnection.CALLBACK_ENUMERATE, cb_enumerate)
    ipcon.register_callback(IPConnection.CALLBACK_CALLBACK_CONNECTED,
                                              cb_connected)
```

Device Identifiers

Every sensor network needs device identifiers. Preferably those identifiers should be unique. Typically a device has some kind of internal indetifier. Here are a few examples of the sensors used in our network:

As it can be seen above, these identifiers do not guarantee to uniquely identify a device within a network. The Tinkerforge id is the weakest, as it is a 32 bit integer (4.294.967.295 options), which might easily collide with another id from a different manufacturer. The tinkerforge id

Device Type	Identifiers	Example
GPIB (SCPI)	**IDN?* returns $manufacturer,$name,$serial,$revision	
Tinkerforge	Each sensor has a base58 encoded integer device id	QE9 (163684)
Labnode	Universal Unique Identifier (UUID)	cc2f2159-e2fb-4ed9-8021-7771890b37ad

is presented as a base58 encoded string. An encoder/decoder example can be found in the TinkerforgeAsync library [8].

The id string returned by a SCPI device is slightly better, but again does not guarantee uniqueness. As it is shown in the example the same device might return a different id defpending on its settings. This typically done by manufacturers for compatibility reasons.

The only reasonably unique id is the universal unique identifier (UUID) or globally unique identifier (GUID), as dubbed by Microsoft, used in the Labnodes. Their id can be used for networks with participant numbers going into the millions.

Calculating the probability of a collision between two random UUIDs is called the birthday problem [40] in probability theory. A randomly generated version 4 UUID of variant 1 as defined in RFC 4122 [24] has 122 bit of entropy, that is out of 128 bit, 4 bit are reserved for the UUID version and 2 bit for the variant. This gives the probability of at least one collision in n devices out of $M = 2^{122}$ possibilities:

$$\begin{aligned} p(n) &= 1 - 1 \cdot \left(1 - \frac{1}{M}\right) \cdot \left(1 - \frac{2}{M}\right) \dots \left(1 - \frac{n-1}{M}\right) \\ &= 1 - \prod_{k=1}^{n-1} \left(1 - \frac{k}{M}\right) \end{aligned} \tag{1.1}$$

Using the Taylor series $e^x = 1 + x \dots$, assuming $n \ll M$ and approximating we can simplify this to:

$$\begin{aligned} p(n) &\approx 1 - \left(e^{\frac{-1}{M}} \cdot e^{\frac{-2}{M}} \dots e^{\frac{-(n-1)}{M}}\right) \\ &\approx 1 - \left(e^{\frac{-n(n-1)/2}{M}}\right) \\ &\approx 1 - \left(1 - \frac{n^2}{2M}\right) = \frac{n^2}{2M} \end{aligned} \tag{1.2}$$

For one million devices, this gives a probability of about 2×10^{-25}, which is negligible.

In the Kraken implementation, all devices, except for the Labnodes, will be mapped to UUIDs using the underlying configuration database. It is up to the user to ensure the uniqueness of the non-UUID ids reported by the devices to ensure proper mapping.

Limitations

There is one inherent limitation to the ethernet bus for instrumentation. The ethernet bus is inherently asynchronous and multiple controllers can talk to the device at the same time. Not only that, but different processes within the same controller can talk to the same device. This makes deterministic statements about the device state challenging.

While it is impossible to rule out the possibility of multiple controllers on a network, care was taken to synchronize the workers within Kraken.

1.3.4. Databases

Cardinality

- TimescaleDB vs Influx
- Example Sensors vs. Experiment

1.4. Short Introduction to Control Theory

This section will give a very brief introduction into some basic concepts of control theory. Many systems require control over one or more process variables. For example, temperature control of a room or a device, or creating a current from a voltage. All of this requires control over a process and is established trough feedback, which allows a controller to sense the state of the system.

The focus of this section lies on the principels feedback and control and will be detailed in the following sections.

1.4.1. Transfer Functions

1.4.2. Open and Closed Loop Systems

To understand feedback, one needs to take a look at dynamical systems. There are two types of systems: open and closed loop systems. A system is called open loop, if the output of a system does not influece its input as in figure 1.1a. On the other hand, if the output is connected to the input of the system it is called closed loop system, an example is shown in figure 1.1b. $G(s)$ is called the transfer function of the system, while $R(s)$ is the input, $Y(s)$ is the output and s the Laplace variable.

(a) Open loop system. (b) Closed loop system.

It is convenient to express the transfer function as its Laplace transform. The unilateral Laplace transform is definded as:

$$\mathscr{L}\left(f(t)\right) = F(s) = \int_0^\infty f(t)e^{-st}\,dt. \tag{1.3}$$

with $f : \mathbb{R}^+ \to \mathbb{R}$, that is integrable and grows no faster than $e^{s_0 t}$ for $s_0 \in \mathbb{R}$. The latter property is important for deriving the rules of differentiation and integration.

To understand the benefits of using the Laplace representation for transfer function a few useful properties must be discussed. First of all the Laplace transform is linear:

$$\begin{aligned}\mathscr{L}\left(a \cdot f(t) + b \cdot g(t)\right) &= \int_0^\infty (a \cdot f(t) + b \cdot g(t))e^{-st}\,dt \\ &= a\int_0^\infty f(t)e^{-st}\,dt + b\int_0^\infty g(t)e^{-st}\,dt \\ &= a\mathscr{L}\left(f(t)\right) + b\mathscr{L}\left(g(t)\right)\end{aligned} \tag{1.4}$$

Another interesting property is the derivative and integral of a function f:

$$\begin{aligned}\mathscr{L}\left(\frac{df}{dt}\right) &= \int_0^\infty \underbrace{f'(t)}_{v'(t)}\underbrace{e^{-st}}_{u(t)}\,dt \\ &= \left[e^{-st}f(t)\right]_0^\infty - \int_0^\infty (-s)f'(t)\,dt \\ &= -f(0) + s\int_0^\infty f'(t)\,dt \\ &= sF(s) - f(0) \end{aligned} \tag{1.5}$$

$$\begin{aligned}\mathscr{L}\left(\int_0^t f(\tau)\,d\tau\right) &= \int_0^\infty \left(\int_0^t f(\tau)\,d\tau e^{-st}\right)\,dt \\ &= \int_0^\infty \underbrace{e^{-st}}_{v'(t)}\underbrace{\int_0^t f(t)\,d\tau}_{u(t)}\,dt \\ &= \left[\frac{-1}{s}e^{-st}\int_0^t f(t)\,d\tau\right]_0^\infty - \int_0^\infty \frac{-1}{s}e^{-s\tau}f(\tau)\,d\tau \\ &= 0 + \frac{1}{s}\int_0^\infty e^{-s\tau}f(\tau)\,d\tau \\ &= \frac{1}{s}F(s) \end{aligned} \tag{1.6}$$

If the initial state $f(0)$ can be chosen to be 0, the differentiation becomes a simple multiplication by s, while the integration becomes a division by s. Finally, the most important aspect is, that a simple relation between the input $r(t)$ and the ouput $y(t)$ of a system can be given. The relation between input and the ouput of a system as shown in figure 1.1a is given by the convolution, see e.g. [6]. Assuming the system has an initial state of 0 for $t < 0$, hence $r(t < 0) = 0$ and $g(t < 0) = 0$, one can calculate:

$$y(t) = (r * g)(t) = \int_0^\infty r(\tau)g(t-\tau)\,d\tau \tag{1.7}$$

Applying the Laplace transformation, greatly simplifies this:

$$\begin{aligned}Y(s) &= \int_0^\infty e^{-st}y(t)\,dt \\ &\overset{1.7}{=} \int_0^\infty \underbrace{e^{-st}}_{e^{-s(t-\tau)}e^{-s\tau}}\int_0^\infty r(\tau)g(t-\tau)\,d\tau\,dt \\ &= \int_0^\infty\int_0^t e^{-s(t-\tau)}e^{-s\tau}g(t-\tau)r(\tau)\,d\tau\,dt \\ &= \int_0^\infty e^{-s\tau}r(\tau)\,d\tau\int_0^\infty e^{-st}g(t)\,dt \\ &= R(s)\cdot G(s) \end{aligned} \tag{1.8}$$

This formula is a lot simpler than the convolution of $r(t)$ and $g(t)$, therefore the use of the Laplace transform has become very popular in control theory.

Another property that is heavily used in control theory is the time delay of functions. To show this property, let $f(t-\theta)$ be

$$g(t) \coloneqq \begin{cases} f(t-\theta), & t \geq \theta \\ 0, & t < \theta \end{cases} \tag{1.9}$$

The reason for this definition is, that the system must be causal. This means, it is impossible to get data from the future ($t < \theta$). An example is shown in figure 1.2a.

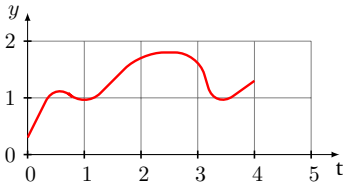

(a) Original signal $f(t)$.

(b) Delayed signal $f(t-2)$.

The Laplace transform of a delayed signal can be calculated as follows:

$$\begin{aligned} \mathscr{L}\left(g(t)\right) &= \int_0^\infty f(t-\theta)e^{-st}\,dt \\ &\overset{1.9}{=} \int_\theta^\infty f(t-\theta)e^{-st}\,dt \\ &\overset{u:=t-\theta}{=} \int_0^\infty f(u)e^{-s(u+\theta)}\,du \\ &= e^{-s\theta}\int_0^\infty f(u)e^{-su} \\ &= e^{-s\theta}F(s) \end{aligned} \tag{1.10}$$

To satisfy the causaulity requirement, the Heaviside function $H(t)$ can be used:

$$\mathscr{L}\left(f(t-\theta)H(t-\theta)\right) = e^{-s\theta}F(s) \tag{1.11}$$

Lastly, the Laplace transform of e^{at}, which is commonly used in differential equations:

$$\mathscr{L}\left(e^{at}\right) = \int_0^\infty e^{(a-s)t}\,dt = \frac{1}{a-s}\left[e^{(a-s)t}\right]_0^\infty = \frac{1}{s-a} \tag{1.12}$$

Using these tools, it is possible calculate the transfer function of a temperature controller. This is done in the next section.

1.4.3. A Model for Temperature Control

In order to describe a closed-loop system, one has to first create a model for the process and the controller involved. A simple model can be derived from the idea, that the system at temperature T_{system} has a thermal capacitance C_{system}, an influx of heat $\dot{Q}_{load}$ from a thermal load and a controller removing heat from the system through a heat exchanger with a resistance of R_{force}. Additionally, there is some leakage through the walls of the system to the ambient environment via $R_{leakage}$. The analogy of thermodynamics with electrondynamics allows to

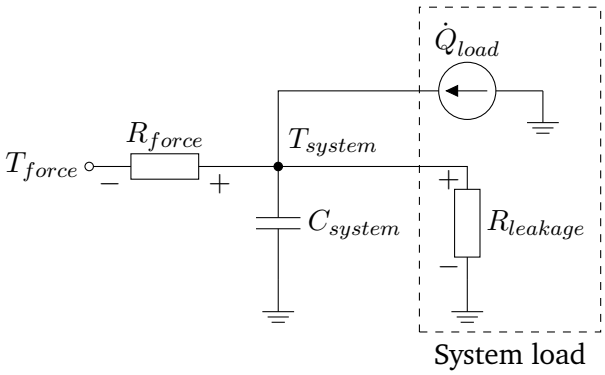

Figure 1.3.: Simple temperature model of a generic system.

create the model in figure 1.3. Since this this model is to be used for a temperature controller, an assumption to simplify it can be made.

The controller will keep T_{system} constant and if the ambient temperature and $\dot{Q}_{load}$ is *reasonably stable*, it is easy to see, that a constant thermal flux must flow through R since it cannot pass through the thermal capacitance C. *Reasonably stable* means that it can be treated as constant with respect to the temperature controller time constants. This will be further discussed in section **??** with regards to system stability. If this assumption holds, the thermal flux from the system load will only cause a constant offset of T_{in}, since the heat must be removed by the controller, and the model can be simplified further:

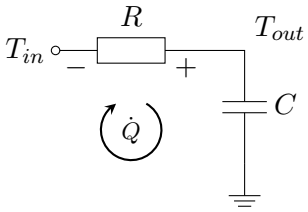

Neglecting the constant thermal flux from the system load and exploiting the analogy of thermodynamics and electrondynamics again, using Kirchhoff's second law, we find:

$$\sum T_i = 0$$
$$T_{in}(t) - \dot{Q}(t)R - \frac{1}{C}\int \dot{Q}(t)\,dt = 0 \tag{1.13}$$

Taking the Laplace transform, applying equation 1.6 and using $T_{out} = \frac{1}{sC}\dot{Q}(s)$ to replace $\dot{Q}$, equation 1.13 can be written as:

$$T_{in}(s) - \dot{Q}(s)R - \frac{1}{sC}\dot{Q}(s) = 0$$
$$\dot{Q}(s) = \frac{T_{in}(s)}{R - \frac{1}{sC}} = \frac{T_{out}}{\frac{1}{sC}}$$

This allows to calculate the transfer function of the process P:

$$\begin{aligned} P(s) = \frac{T_{out}}{T_{in}} &= \frac{\frac{1}{sC}}{R - \frac{1}{sC}} \\ &= \frac{1}{sRC + 1} \\ &= \frac{K}{1 + s\tau} \end{aligned} \tag{1.14}$$

with the system gain K and the time constant τ. In case of the RC circuit, the gain is 1, but other systems may a gain or attenuation of $K \neq 1$ in the sensor.

Equation 1.14 is called the transfer function of a first-order model, because its origin is a differential equation of first order. This model describes homogeneous systems, like a room, very well, as can be seen in section **??**, but in order to derive the transfer function including the controller and the sensor some more work is required.

Expanding on figure 1.1b and equation 1.7 the closed-loop transfer function becomes:

$$G(s) = P(s) \cdot S(s) \tag{1.15}$$

and the block diagram becomes

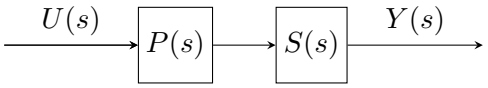

Figure 1.4.: Open loop system with sensor.

The transfer funciton of the sensor can, in the most simple case, be modeled as a delay line with delay θ and $f(t - \theta) = H(t - \theta)$. Using equation 1.10 $S(s)$ can be written as

$$S(s) = e^{-\theta s}. \tag{1.16}$$

The full process model including the time delay is:

$$G(s) = \frac{K}{1 + s\tau} e^{-\theta s} \tag{1.17}$$

This is called a first-order plus dead-time model (FOPDT) or first-order plus time-delay model (FOPTD). To fit experimental data to this model it is more convenient to transform the transfer function 1.17 into the time domain. To calculate the output response an input $U(s)$ is required. In principal any function can do, but a step function is typically used, for example by Ziegler and Nichols [44] and many others [29, 32, 39, 38, 36, 37, 6]. It is both simple to calculate and apply to a real system. Using equations 1.10 and 1.12, the Heaviside $H(t)$ step function transforms as

$$\mathscr{L}\left(u(t)\right) = U(s) = \mathscr{L}\left(\Delta u H(t)\right) = \frac{\Delta u}{s} \tag{1.18}$$

with the step size Δu. The output $Y(s)$ can then be calculated analytically.

$$
\begin{aligned}
Y(s) &= \frac{\Delta u}{s}\frac{K}{1+s\tau}e^{-\theta s} \\
&= K\Delta u\frac{1}{s(1+s\tau)}e^{-\theta s} \\
&= K\Delta u\left(\frac{1}{s}-\frac{\tau}{s\tau+1}\right)e^{-\theta s} \\
&= K\Delta u\left(\frac{1}{s}-\frac{1}{s+\frac{1}{\tau}}\right)e^{-\theta s}
\end{aligned} \tag{1.19}
$$

To derive $y(t)$, the inverse Laplace transform of $Y(s)$ is required. Unfortunately, this is not as simple as the Laplace transform. Fortunately, using 1.12 while making sure causaulity is guaranteed as shown in 1.11, the simple first order model can easily be transformed back into the time domain.

$$
\begin{aligned}
\mathscr{L}^{-1}\left(Y(s)\right) = y(t) &= K\Delta u\mathscr{L}^{-1}\left(\frac{1}{s}e^{-\theta s}\right) - K\mathscr{L}^{-1}\left(\frac{1}{s+\frac{1}{\tau}}e^{-\theta s}\right) \\
&\overset{1.12}{=} K\Delta u\cdot 1\cdot H(t-\theta) - \left(e^{-\frac{t-\theta}{\tau}}\right)H(t-\theta) \\
&= K\Delta u\left(1-e^{-\frac{t-\theta}{\tau}}\right)H(t-\theta)
\end{aligned} \tag{1.20}
$$

The time domain solution of the FOPDT model can now be used extract the parameters τ, θ and K from a real physical system using a fit to the measurement data. The parameter Δu is already known, since it is an input parameter. A simulation of the step response of a first-order model with time delay is shown in figure 1.5. Here it can be clearly seen, that the output does not change until the time delay θ has passed and the Heaviside function changes from 0 to 1.

1.4.4. PID tuning rules

We use $\tau_c = \tau$ as suggested by [39, 38] for "*tightest possible subject to maintaining smooth control*".

1.5. Allan Deviation

The Allan variance [4] $\sigma_y^2(\tau)$ is a two-sample variance and used as a measure of stability. The Allan deviation $\sigma_y(\tau)$ is the square root of the variance. Originally, the Allan variance was used to quantify the performance of oscillators, namely the frequency stability, but it can be used evaluate any quantity. In order to define the Allan variance, a few terms need to be defined first. A single measurement value of the time series $y(t)$ can be written as

$$
\bar{y}_k(t) = \frac{1}{\tau}\int_{t_k}^{t_k+\tau} y(t)\,dt. \tag{1.21}
$$

This is the k-th measurement with a measurement time or integration time τ. The latter term is frequently used for DMMs. t_k is the sampling inverval including the dead time θ

$$
t_{k+1} = t_k + T \tag{1.22}
$$

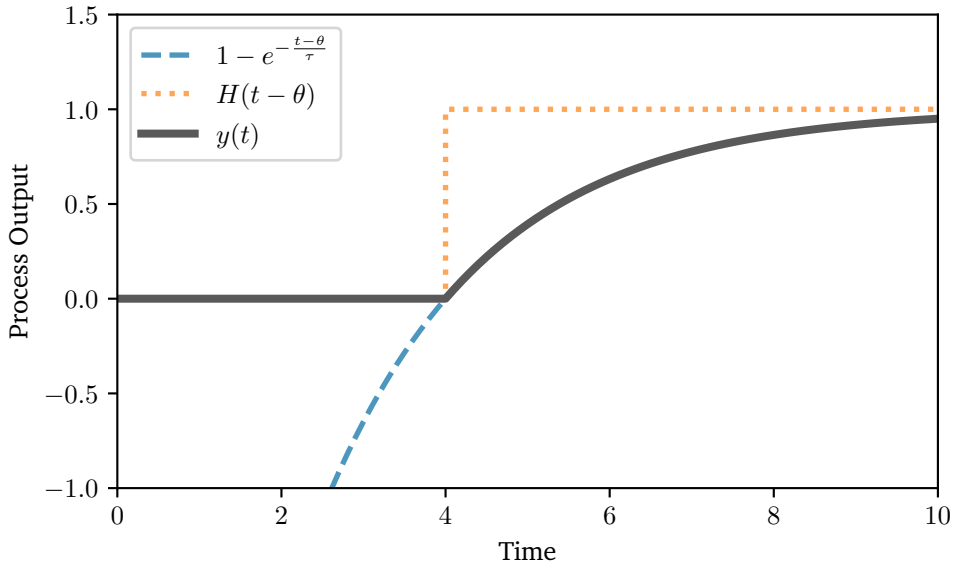

Figure 1.5.: Time domain plot of a first-order plus dead time model, showing induvidual components of the model and the composite function $y(t)$. Model parameters: $K = \Delta u = 1, \tau = 2, \theta = 4$.

with

$$T = \tau + \theta. \tag{1.23}$$

Using this, the standard deviation over N sampled is defined as [4, 7]

$$\sigma_y^2(N, T, \tau) = \left\langle \frac{1}{N-1} \left(\sum_{n=0}^{N-1} \bar{y}_n^2(t) - \frac{1}{N} \left(\sum_{n=0}^{N-1} \bar{y}_n(t) \right)^2 \right) \right\rangle \tag{1.24}$$

The $\langle\ \rangle$ denotes the (infinite time) average over all measurands y_k. Hence for all k.

The Allan variance is a special case of this definition with zero dead-time ($\theta = 0$) and only 2 samples:

$$\sigma_y^2(\tau) = \sigma_y^2(N = 2, T = \tau, \tau) \tag{1.25}$$

$$= \left\langle \frac{\left(\bar{y}_{k+1} - \bar{y}_k\right)^2}{2} \right\rangle \tag{1.26}$$

In practice, no experiment can take an infinite number of samples, so typically the Allan variance is estimated using a number of samples m:

$$\sigma_y^2(\tau) \approx \frac{1}{m} \sum_{k=1}^{m} \frac{\left(\bar{y}_{k+1} - \bar{y}_k\right)^2}{2} \tag{1.27}$$

It can be shown [7], that 1.27 is indeed more usefull than $\sigma_y^2(N \to \infty, T = \tau, \tau)$, becuase $\sigma_y^2(\tau)$ even for $m \to \infty$ converges for processes, that do not have a convergent $\sigma_y^2(N \to \infty, T = \tau, \tau)$.

Additionally, the Allan variance is mathematically related to the two-sided power spectral density $S_y(f)$ [7]:

$$\sigma_y^2(\tau) = 2\int_0^\infty S_y(f)\frac{\sin^4(\pi f t)}{(\pi f \tau)^2}\,df \tag{1.28}$$

and therefore all processes, that can be seen in the power spectral density can also be seen in the allan deviation. The inverse transform, however, is not always possible as shown by Greenhall [13].

Distinguishing different noise processes using the Allan deviation will be elaborated in the next section.

1.5.1. Identifying Noise in Allan Deviation Plots

It was already mentioned by Allan in [4], that types of noise, whose spectral density follows a power law

$$S(f) = C \cdot f^\alpha \tag{1.29}$$

can be easily identified in the Allan deviation plot. The most common power coefficients encountered in experimental data can be found in table 1.1 and warants a further discussion.

Amplitude noise type	Power-law coefficient α	Allan deviation	$\sigma_y(N=2, T=\tau+\theta, \tau)$
White noise	0	$\propto \tau^{-1/2}$ [5]	
Flicker/Burst noise	-1	$\propto \tau^{0}$ [5]	
Random walk noise	-2	$\propto \tau^{1/2}$ [5]	
Drift	–	$\propto \tau^{1}$ [14]	

Table 1.1.: Power law representations using the Allan variance.

In the previous section in equation 1.25, the Allan deviation was defined as the two-sample variance without dead-time. The effect of dead-time will be discussed later. The more important aspect is the general shape of the Allan deviation of the different power laws and will be discussed first. Linear drift, which can not be considered noise, but deterministic process has a very characteristic shape in the Allan deviation plot and will therefore be discussed here as well.

White Noise

White noise is probably the most common type of noise found in measurement data. Johnson noise found in resistors, caused by the random fluctuation of the charge carriers, is one example of mostly white noise up to bandwidth of 100 MHz, from where on quantum corrections are required [12]. Amplifiers also tend to have a white noise spectrum at higher frequencies. For these reasons, white noise typically makes up for a considerabe amount of noise in a measurement, unless one measures at very low frequencies. White noise is a series of uncorrelated random events and therefore characterised by a uniform power spectral density, which means there is the same power in a given bandwidth at all frequencies. Another one of its important and often used properties is, that the variance of two uncorrelated variables adds:

$$\sigma_{x+y}^2 = \sigma_x^2 + \sigma_y^2 + \underbrace{2\,\mathrm{Cov}(x,y)}_{\text{uncorrelated}=0} = \sigma_x^2 + \sigma_y^2 \tag{1.30}$$

This allows the simple addition of variances from different sources, but it must be stressed here, that this property is only valid for uncorrelated sources like white noise, although it is usually incorrectly applied to all measurements in disreagard of the dominant noise present. This Unfortunately obscures rather than clarifies the uncertainties involved.

In order to demonstrate the effect of white noise in Allan deviation plots, it was simulated using Python and the excellent AllanTools library [42]. The noise generator chosen in the AllanTools library is based on the work of Kasdin and Walter [17]. The full Python program code is published online []. For better comparison, all noise densities are normalized to give an Allan deviation of $\sigma_y(\tau_0) = 1$.

Figure 1.6 shows a sample of white noise in three different forms. Figure 1.6a is the time series representation. From this sample, the power spectral density was calculated and is shown in figure 1.6b. The dashed line shows the expectation value of the power spectral density and the Allan deviation.

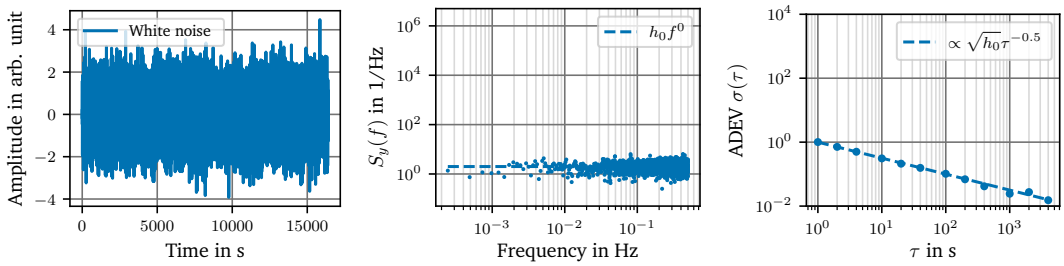

(a) Time domain (b) Power spectral density (c) Allan deviation

Figure 1.6.: Different representations of white noise.

From this simulation, several features can be observed. First of all, the power spectral density is flat and constant with $h_0 = 2$, which is in accordance with table 1.1 and the normalization mentioned earlier. Figure 1.6c shows the typical $\tau^{-\frac{1}{2}}$ dependence of white noise in the Allan deviation plot. This immediatly explains, why filtering white noise scales with $\frac{1}{\sqrt{n}}$ with n being the number of samples averaged.

Burst Noise

Burst noise, popcorn noise, or sometimes referred to as random telegraph signal is a random bi-stable change in a signal and is caused by a generation recombination processes. This, for example, happens in semiconductors if there is a site, that can trap an electrons for a prologned period of time and then randomly release it. Imporities causing lattice defects are discussed in this context [20, 33, 9, 19]. Such latttice defects can also be introduced by ion implantation during doping.

The discussion is split into two parts. First the power spectral density is derived and then the Allan variance. The spectral density of burst noise caused by a single trap site was derived in [28] by Machlup. The author used the autocorrelation function of the burst noise signal and applied the Wiener-Khinchin (Wiener-Хи́нчин) theorem, which connects the autocorrelation function with the power spectral density. A nicely detailed derivation can be found in [43], which also discusses the preconditions, that must be met, like stationarity of the process. The burst noise signal consists of two energie levels, called 0 and 1, split by Δy. Multiple burst noise signals can be superimposed in a real device. This would then result in mutiple levels, but they can be treated separately. The measurement interval over an even number of transitions, so that one ends in the same state as the measurement has started, is the time T. The mean

lifetime of the levels is called $\bar{\tau}_0$ and $\bar{\tau}_1$:

$$\bar{\tau}_0 \approx \frac{1}{N}\sum_i^N \tau_{0,i} \qquad \bar{\tau}_1 \approx \frac{1}{N}\sum_i^N \tau_{1,i} \tag{1.31}$$

Figure 1.7 shows a burst noise signal along with the definitions above.

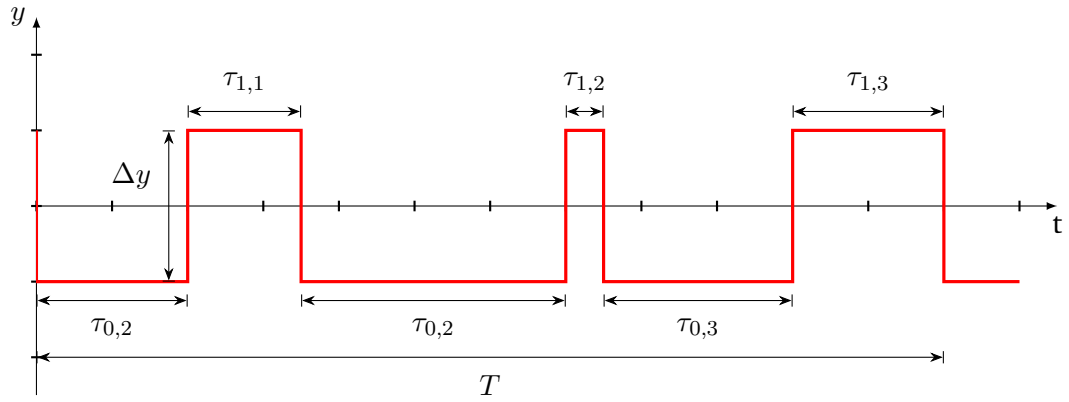

Figure 1.7.: A random burst noise signal.

Using these definitions, one can then derive [28]:

$$R_{xx}(T) = (\Delta y)^2 \cdot \frac{\bar{\tau}_1\bar{\tau}_0 e^{-\left(\frac{1}{\bar{\tau}_1}+\frac{1}{\bar{\tau}_0}\right)T}}{\left(\bar{\tau}_1+\bar{\tau}_0\right)^2} \text{ and} \tag{1.32}$$

$$S(\omega) = 4R_{xx}(0)\frac{\frac{1}{\tau_1}+\frac{1}{\tau_0}}{1+\omega^2\left(\frac{1}{\bar{\tau}_1}+\frac{1}{\bar{\tau}_0}\right)^2} \qquad \omega > 0. \tag{1.33}$$

Note, that the power spectral density is the one-sided version, hence an additional factor of 2 is included. The d.c. term was ommitted here and can usually be neglected, because it is not relevant for calculating the power spectral density of real measurement data as it only contributes a single peak at $\omega = 0$. Using $\frac{1}{\bar{\tau}} = \frac{1}{\bar{\tau}_1} + \frac{1}{\bar{\tau}_0}$ equation 1.33 can be rewritten to give a more intuitive form:

$$S(\omega) = 4R_{xx}(0)\frac{\bar{\tau}}{\omega^2+\bar{\tau}^2} \tag{1.34}$$

This is a Lorentzian function and it can be seen, that a single trap site has a power spectral density that is proportional to $\frac{1}{f^2}$ at higher frequencies and it is also immediately evident, that for low frequencies, the power spectral density must be flat.

With the spectral density in hand, it is now possible to calculate the Allan variance as it was done by

This type of noise has become less prevalent in modern manufacturing processes, because the quality of the semiconductors has improved. But if, for example a trap site is located very close to an important structure, for example a high precision Zener diode, its effect might be so strong, that it can be clearly seen.

The small wiggles at longer τ are typical end-of-data errors caused by spectral leakage, because there are insufficient samples to average over [16]. As it was discussed above, the Allan deviation can only be estimated given a limited number of samples using equation 1.27. This leads to the fact, that at $\frac{\tau}{2}$ there are only 2 samples left, so there no averaging possible to

improve the estimate of the Allan deviation. This leads to oscillations at low frequencies or large τ.

The coefficients given here are using the assumption, that the Allan deviation is the appropriate measure for the sample data. This might not always be the case, because the Allan deviation assumes a dead time of $\theta = 0$. This problem was extensively discussed by Barnes et al. [7] and even special models were developed to account for the algorithms of modern frequency counters [10]. It is therefore important to discuss typical measurement settings for voltmeter to estimate errors that arise from those settings. Typical settings, that affect the dead time of a voltmeter are auto-zeroing and line synchronization. Auto-zeroing is typically done by adding additional measurements to the normal input integratiion cycle. These measurements are a zero measurement to correct for offset drift and a measurement of the reference voltage to correct for gain errors. The implementation details and type of measurements are manufacturer dependant and must be determinded for every multimeter used.

1.6. Temperature Controller

1.6.1. Tuning of a PID controller

The number of emperical algorithms to determine a set of PID parameters (K_p, K_i, K_d) are numerous. In this work only the most common algorithms and a few notable exceptions will be presented.

1.6.2. Design

2. Results

2.1. Laser Current Driver

2.1.1. Zener Diode Selection

Early tests of the LM399 Zener diode as a reference have confirmed, what the data sheet [26] already suggest in the 'Low Frequency Noise Voltage' plot. There are random bi-stable voltage step changes. This phenomenon is called burst noise or popcorn noise.

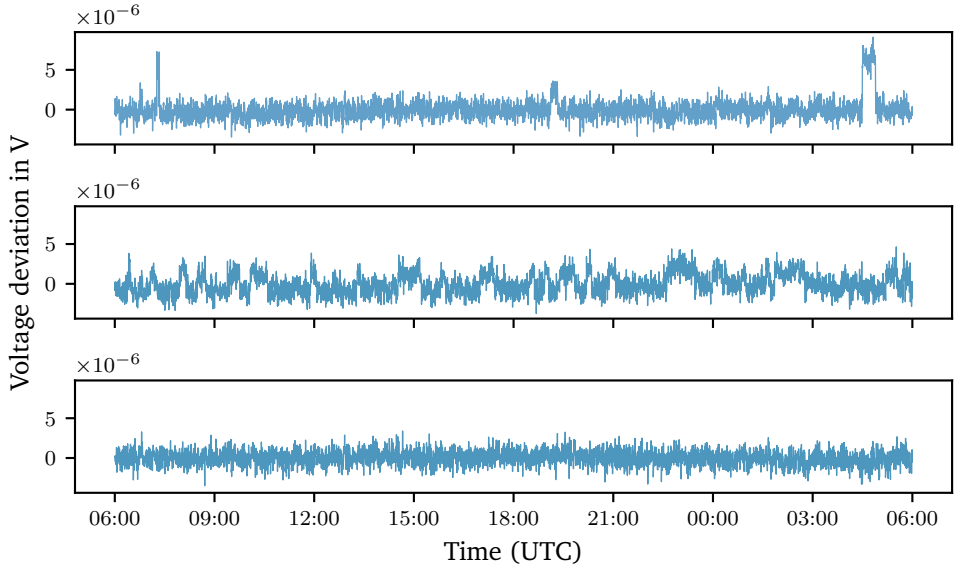

Figure 2.1.: Popcorn noise in different samples of the LM399 over a 24 h period.

Figure 2.1 shows two samples of the LM399, that exhibit popcorn noise, while the last one does not.

The sources of popcorn noise in semiconductor devices are not yet fully understood, but some sources have been identified. Defects in the semiconductor crystal lattice and contamination of the semiconductor material have been linked to popcorn noise [19]. This problem has improved over the years as manufacturing processes and wafer quality has evolved. Unfortunately the LM399 is built around a process from 1991, as can be seen etched into the die [18].

The popcorn noise caused by defects and contamination can be reduced by lowering the strain on the lattice and removing surface contaminants on the die. This can be can be achieved using a high-temperature burn-in process. Manufacturers like Fluke and Keysight use similar techniques in their products. Fluke, for example, uses a period of 60 d burn-in for their references [34].

Fortunately, the LM399 is a heated reference, which regulates its die to 90 °C when turned on, so it is only required put the diodes in a simple test circuit and wait. The use of a separate test setup instead of the final circuit has both advantages and disadvantages. The disadvantage is, that the Zener diode will subjected to mechanical stress when soldered, this stress will not be removed by the burn-in process as it happens after the testing, when diode is soldered into the final circuit, but this mainly affects the voltage drift properties of the Zener diode and not the popcorn noise. The drift of the diode is also only of secondary concern in our setup, as the drift is mainly caused by the reference resistors used and are typically at least an order of magnitude worse than the the drift of the diode judging by the data sheet [26, 41].

The advantages of testing the Zener diodes separately, on the other hand, are, that more diodes can be tested at the same time, as a special compact test fixture can be used. It is also simpler to remove the diodes from the test fixture, because they be socketed. Therefore for our application a separate test board was used. Building this test setup is detailed in the next sections.

2.1.2. Building a Test Setup for Zener Diodes

There are several ways to measure the popcorn noise of semiconductor devices. The most trivial one is to directly monitor the device in the time-domain. In this case, the Zener voltage can be monitored with a long-scale multimeter. It requires a low noise DMM, that can reliably distinguish between both voltage levels, which are about 4 µV apart. A related option is to use a second reference, whose voltage is similar to the device under test (DUT). Measuring the the voltage difference between the two references, less resolution is required. Directly comparing the difference of two references using a millivolt meter is commonly done when intercomparing primary voltage references. This method, however, increases the measurement noise by a factor of $\sqrt{2}$, if both references produce the same level of uncorrelated noise. The noise of the LM399 with a 100 PLC integration time (2 s) is about 1.5 μV_{pp} as can be determined from the data in figure 2.1.

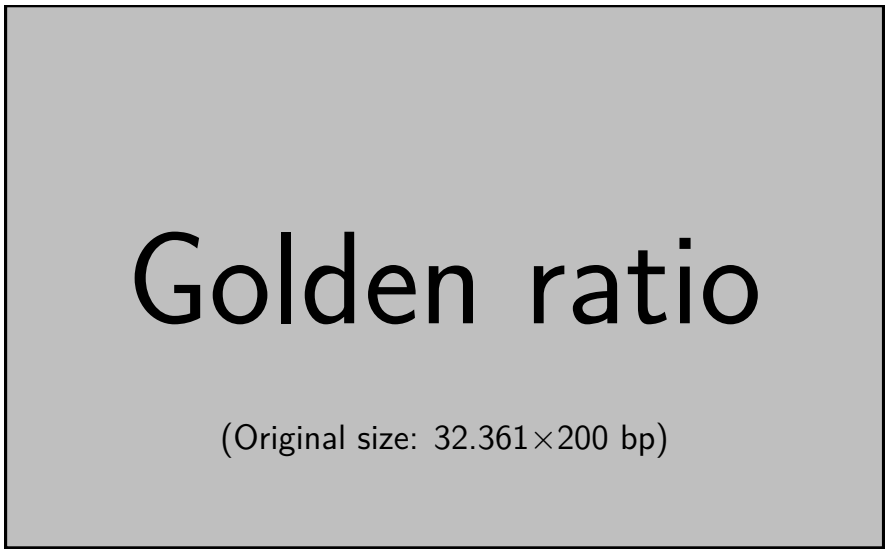

Figure 2.2.: Voltage noise of an LM399, measured with a bandwidth of 0.1 Hz−10 Hz.

Measuring two references against each other would then result in around 2.1 µV of noise. This make distinguishing the jumps possible, but challenging.

A third option is to use a high-pass filter and an amplifier. Additionally, the signal can be low-pass filtered to remove any excess high frequency noise. This approach also requires less resolution than directly measuring the voltage, because the signal-to-noise-ratio is improved du the amplifier. It is therefore possible to use an off-the-shelf analog-to-digital converter (ADC). One such circuit, along with some examples, is demonstrated in [19, 20]. It must be noted, that due to the high-pass filtering, it not possible to measure slow voltage drifts using this method.

The forth and final option presented here, is approaching the problem in the frequency domain and requires a low-noise amplifier with a low frequency cutoff. As it was already discussed in section **??**, popcorn noise is found to have a frequency dependence of $1/f^2$. This can be used to distinguish it from other random noise processes that show a frequency dependence of $1/f$. An good example is given in Horowitz and Hill in *The Art of Electronics* on page 478 [15]. Going to frequencies below 10 Hz, one can sort the references by their noise spectrum.

In this work only options one and two were were tested, as it was said above, with options three and four there is a chicken and egg problem. One needs a number on known good devices to compare other DUTs to. At the start of the evaluation, most of the data available about the LM399 was from the data sheet. Compiling a dataset of the performance of dozens of LM399 is expensive and time consuming and companies typically treat such data as a closely guarded secret.

The next section deals with the choice of multimeter to satisfy the requirements test the Zener diodes according to options one and two, so either directly measuring the output voltage or difference of a known good sample against the DUT.

2.1.3. Choosing a Multimeter for Testing Zener Diodes

The DMM used plays an important role for the test setup. In this section, some of the challenges, that can be encountered will be discussed. The expected amplitude of the popcorn noise is around 0.5 µV/V or 3.5 µV of the output voltage, when considering the 7 V Zener voltage of the LM399 diode.

The 7 V will typically be measured on the 10 V range. It is not a trivial task, because a signal-to-noise-ratio of 0.35 µV/V or more than 130 dB is required. This calls for a device, that not only has the required resolution, but also the stability over time and temperature to ensure the measurement will not be distorted by the DMM.

Therefore, a voltmeter with lower noise and a more stable reference, than the DUT is mandatory. This only leaves the class of very low noise 7.5 or 8.5 digit multimeters. These multimeters feature a different type of voltage reference, because the LM399 is not suitable due to its noise. The only Zener diodes that meet those requirements are the Analog Devices LTZ1000 [27], the Motorola SZA263 (out of production) and the Linear Technology (LT) LTFLU-1, a proprietary design by Fluke and LT. The LTZ1000, for example, is specified for a typical noise of 1.2 μV_{pp} in a frequency range of 0.1 Hz–10 Hz [27]. Additionally, in comparison to the LM399, those Zener diodes do not suffer from the popcorn noise issue.

The equipment manufacturers typically have a preference for one of those diodes. Keysight utilizes the LTZ1000, Fluke uses the SZA263 (in older devices) or the LTFLU-1 in newer model, while Keithley employs the LTZ1000 in their `Model 2002` and the LTFLU-1 in the newer `DMM7510`, because they were bought by Fortive, the same company that owns Fluke. To sum it it up, Keysight uses the LTZ1000 and Fluke/Keithley the LTFLU-1 in their top end meters.

Comparing only 7.5 and 8.5 digit voltmeters, narrows down the choice of multimeters considerably. The market for high-end 8.5 digit DMMs is limited and therefore every device on the market caters for a certain niche. It is therefore prudent to look at their specifications to choose the correct device for this purpose. In table 2.1 a list of popular 8.5 DMMs can be found. Several models included in the table, are already discontinued, but these DMMs can still be acquired on the second-hand market.

Manufacturer	Model	Remarks
Advantest	R6581	Discontinued. Scanner cards available.
Datron/Wavetek	1812	Discontinued. Wavetek was bought by Fluke.
Fluke	8508A	Discontinued. 20 V range.
Fluke	8588A	In production.
Keithley/Tektronix	2002	In production. Scanner card available. 20 V range.
Keysight	3458A	In Production.
Solartron	7081	Discontinued. Slow.
Transmille	8104	In Production. External scanner available. Slow.

Table 2.1.: Overview of 8.5 digit multimeters.

While the author has not tested every multimeter in table 2.1, it is possible to judge some of them apriori by their specifications. The Solartron 7081 (also sold as Guildline 9578) is a less optimal choice, because a conversion takes 52 s for 8.5 digits. The discontinued Fluke 8508A and the Wavetek 1812 multimeter are very similar devices, because Fluke bought Wavetek in 2000 and as a result, the Fluke 8508A is more of an update to the Wavetek 1812 than a new device. They are both in included in the list, because it is very rare to see one of the Fluke devices on the second hand market, while the Wavetek 1812 can be found with a bit of patience. Again they are fairly slow, taking 25 s for a conversion at 8.5 digits.

The other multimeters are still in production and similar in price, but their field of use is slightly is different. The Fluke 8588A excels at stability and features a modern user interface, whereas the Keysight 3458A is unbeaten in linearity and noise. A detailed comparison of those two meters can be found in the work of Lapuh et al. [23]. The Keithley Model 2002 focuses on its scanning capability and the Transmille 8104 does have electrometer functions. Unfortunately, the 8104 is also fairly slow at 8.5 digit with conversions taking 4 s at its fastest setting [2], so it will not be considered.

To narrow it down even further, several 7.5 and 8.5 digit multimeters were tested. The results of those tests will be discussed here to give an impression of the performance of these devices. The tested multimeters are the Keysight 3458A, the Keithley Model 2002, the Keysight 34470A and a Keithley DMM6500. The 3458A was chosen, because it is very fast and already used in section **??** of this work. The Model 2002 was chosen for its internal scanning unit. The 34470A was chosen as a lower-end and cheaper alternative and because it is a fairly low noise device. Finally the DMM6500 is on the list to compare a DMM with an LM399 reference. A Fluke 8588A was not tested, because it was not released at the time of testing and the older model 8508A is considered too slow as mentioned above.

The tests

Two test were run on this selection of devices. The first one was done using a Fluke 5440B calibrator supplying 10 V to all mulimeters and taking readings over the course of a week. This data was used to estimate the noise and the stability of the multimeters, including burst noise. The noise of the DMM at 10 V is typically not found in the datasheet, because the noise

performance is usually quoted for shorted inputs, which does not include the internal reference noise. This test allows to check for popcorn noise of the internal reference. The calibrator has a specified output noise of $<1.5\,\mu V$ within a bandwidth of 0.1 Hz–10 Hz at 1 V and is stable to within $5\,\mu V_{RMS}$ over 30 d, a specification far superior to the LM399.

The second test was done using a known bad LM399 voltage reference instead of the calibrator. This test was done to see how well a DMM can make out the popcorn noise.

Based on these two tests, a multimeter was chosen for an automated test setup to bin the LM399s.

Test Setup

The tests were done in a stable and monitored lab environment, with a temperature deviation of at most $\Delta T = \pm 0.2\,K$. All multimeters were connected to the same DUT. Although this might potentially cause interference between the multimeters due to the pump out current spikes caused by the switching interals, no ill effects, like voltage offsets or increased noise, were observed during the setup of the tests. A more detailed discussion of the pump out current of the `3458A` can be found in [35].

The three 8.5 and 7.5 digit multimeters were connected using shielded cables, either Pomona 1167-60 or self-made cables. See section **??** for details on the self-made cables. The GUARD terminal of the calibrator was connected to chassis GROUND at the calibrator and then connected to the cable shield. On the `3458A`, the shield was connected to the GUARD terminal and the GUARD switch was set to open according to the manual [22]. For the other multimeters, that do not have a GUARD terminal, the shield was left floating at the DMM side. Additionally the `Fluke 5440B`, the `HP 3458A` and the `Keysight 34470A` have an autocalibration routine, which was run once prior to the measurement. The detailed settings used for the DMMs can be found in the appendix A.1 on page 35, a summary ist given in table 2.2 to show the important differences.

DMM	Integration time in NPLC	Conversion time in s
`HP 3458A`	100	0 s
`Keithley Model 2002`	40	0 s
`Keysight 34470A`	100	0 s
`Keithley DMM6500`	90	0 s

Table 2.2.: Concise list of differences in the settings used for comparing the DMMs.

All DMMs were configured to have a similar conversion time. This lead to different integration times, which are given in power line cycles at 50 Hz. The `Model 2002` takes considerable longer for a measurement than the Keysight multimeters. The reason is the auto-zero function, which is shown in figure **??**. The `Model 2002` does three steps when doing auto-zeroing, it measures the signal, the zero point for an offset compensation and also the reference voltage for a gain correction. In comparison, the `3458A` only corrects for the offset drift. The gain is adjusted when using the ACAL function. The former auto-zero routine, therefore takes longer by one half, but results in more stable measurements.

These measurements were done by measuring the output voltage of a pre-production version of the reference PCB for the digital current driver. The reference board was kept at 23 °C in a custom thermal chamber. The chamber is detailed in section **??**. Additionally, a 500 g bag of Bentonite desiccant was added to keep the references at a low humidity of around 20 % relative humidity. The reference board inserted into a motherboard holding up to 4 reference modules.

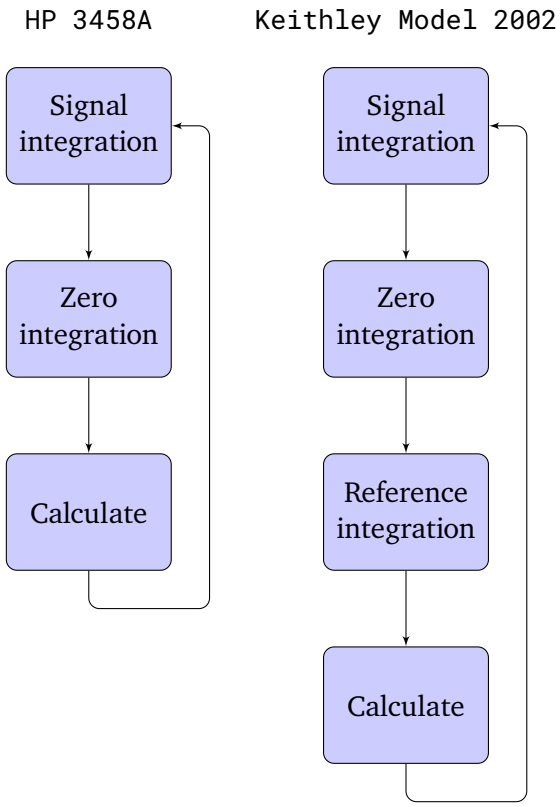

Figure 2.3.: Auto-zero phases of the HP 3458A and Keithley Model 2002.

The motherboard, also called LM399 breakout board, provides the voltage regulators and the operational amplifier for the kelvin sensed pins of the reference. The multimeter was directly connected to the reference via a DB9 connector, without an other components in between the reference and the DMM like buffers, multiplexers or filters. The DMM itself was exposed to the ambient temperature of the lab. The setup is shown in figure 2.4.

The reference boards amplify the Zener voltage to 10 V, which improves the signal to noise ratio, because it makes use of the full DMM range. The 10 V range is typically the lowest (relative) noise and lowest drift range those multimeter because no internal pre-amplifiers of attenuators are required. It is important to keep the temperature drift of the DMM low or at least predictable, because the device is exposed to the ambient laboratory and not in a temperature controlled environment like the references.

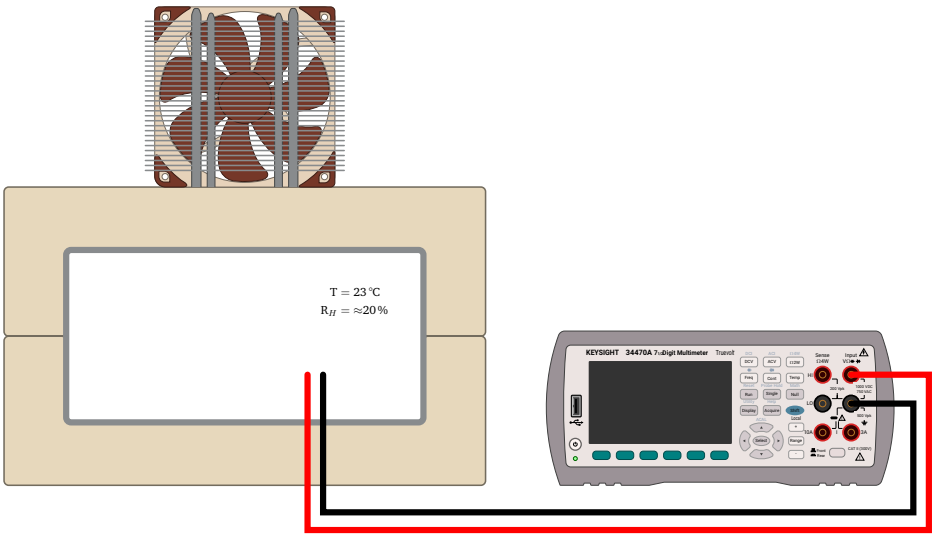

Figure 2.4.: Measurement setup for tesing an LM399 reference board with the `Keysight 34470A`

The reference is a negative 10 V reference that uses a self-biasing technique to derive its 1 mA Zener current from its own −10 V output. The details of this circuit are discussed in section **??**.

With the amplified output the expected burst noise step size of about 0.5 µV/V, becomes 5 µV. The resolution of the 10 V range of the `34470A` is 100 nV, but the measurement is not limited by quantization. See section **??** of this work for a detailed characterization.

Figure 2.5 shows an example of such measurement. This measurement highlights one the problems encountered during those measurements. From this measurement it is unclear whether the features seen in the graph are only a result of ambient temperature changes due to the cycling of the air conditioning or popcorn noise on top of that. These results hightlight the fact, that sub-ppm measurements not only requires high-end gear, but also a very stable environment. From the data it follows, that the temperature coefficient of the DMM in linear approximation is:

$$\alpha_{\texttt{34470A}} \approx \frac{6.08\,\mu\text{V} - (-9.30\,\mu\text{V})}{(21.85\,^\circ\text{C} - 19.96\,^\circ\text{C})10\,\text{V}} = 0.86\,\mu\text{V}/(\text{V}\,\text{K}) \tag{2.1}$$

While the temperature coeeficient is vastly better than the specified 2 µV/(V K) [11], it is not low enough for this type of measurement. The multimeter must therefore be kept in a temperature controlled environment. This issue was resolved by replacing the stock air conditioning controller with a custom PID controller as discussed in section **??**. Lastly, the noise floor of the measurement is 1.5 μV_{RMS}, resulting in an estimated signal-to-noise ratio (SNR) of about 10 dB, which is suffient to detect the popcorn noise.

While the temperature issue was being worked on, testing of the Zener diodes continued. To work around the temperature drift of the DMM, the amplification of the reference voltage was increased to 15 V, the same voltage required by the digital current driver, and a differential measurement was realized. This measurement was done against a primary 15 V reference board. To ensure, that any popcorn noise found originates only in the DUT and not the primary reference used, several reference boards where tested against a `Fluke 5440B`. The `5440B` does not exhibit popcorn noise as it uses a different voltage reference ic, namely two Motorola

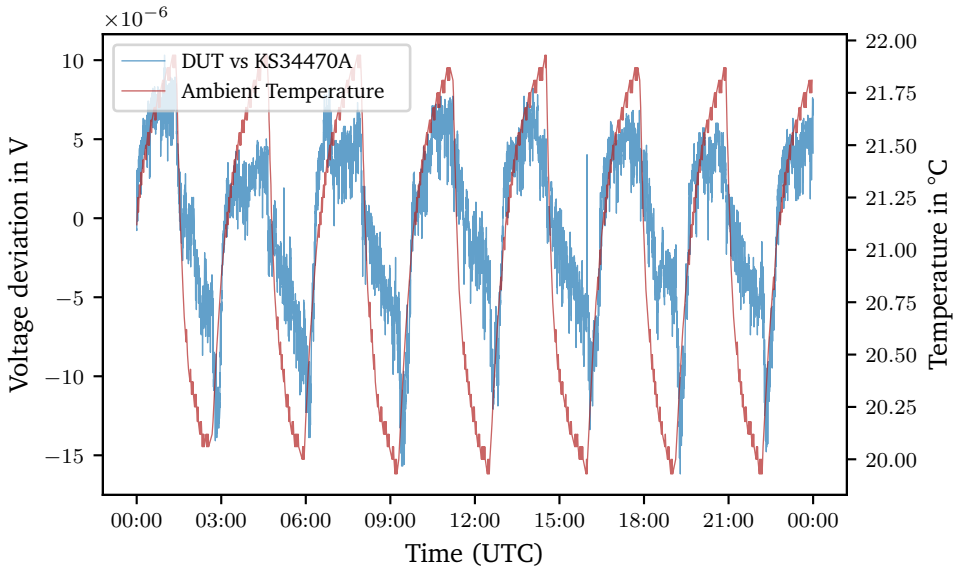

Figure 2.5.: Voltage deviation from the mean voltage of a LM399 negative 10 V reference measured with a Keysight 34470A at 100 PLC.

SZA263 in series [1]. Finally, a board that did not show popcorn noise in a period of three days was selected. The serial number of this primary or golden reference is *#1*.

Using this differential technique, the results greatly improved

In order to test a large amount of Zener diodes, and considering the duration of the burn-in process, which can take anything between 100 h–1000 h, it is necessary to have an automated setup. This consists of a digital multimeter (DMM) a scanner and test board, that holds the Zener diodes and provides the necessary infrastructure for the diodes.

To conclude, we need a high performance DMM, a scanner, and a test fixture. The choices will detailed in the following sections.

2.1.4. A Scanner System for Testing Zener Diodes

As discussed before the diodes need to be tested for 1000 h and it is not be feasible to test them individually. So a minimum of 10 diodes must be tested at the same time. To keep the system compact, the test setup a scanner to multiplex a single multimeter input. Several commercial options currently available were considered for this project and are shown in table 2.3.

A recent trend to more compact devices has led major manufacturers to include multimeters in the scanner mainframe creating so called data acquisition units. Legacy devices, that only have switching capabilities are no available. For example Keithley replaced the small desktop switch mainframe `Model 7001` with the `DAQ6510` and Keysight is offering the `DAQ973A`, a scanning 6.5 digit DMM, that accepts extension cards. Unfortunately, for this project, as discussed above, the integrated 6.5 digit multimeter does not add any value.

The simplest option is to go with an 8.5 digit multimeter that already included a scanner option or buy a used `Keithley 7001` from a second-hand dealer. The author has tested both options and the simplicity of only having a single device to connect and program makes the integrated scanner card of the `Model 2002` very attractive.

	Keysight		Keithley			Fluke	Rigol
	DAQ973A	34980A	DAQ6510	2750	3706	2680	M300
DMM	6.5	6.5	6.5	6.5	7.5	18 bit	6.5
Channels	3x20	8x40	2x10	5x20	6x60	6x20	5x32
FET	✓	✓	✓	✓	✓	✗	✗
Voltage	120 V	80 V	60 V	60 V	200 V	75 V	300 V
Card	DAQM900A	34925A	7710	7710	3724	2680A-PAI	MC3132
USB	✓	✓	✓	✗	✓	✗	✓
Ethernet	✓	✓	✓	✗	✓	✓	✓
GPIB	✓	✓	✓	✓	✓	✗	✓

Table 2.3.: Overview of scanner mainframes

The scanner card used to multiplex the DMM does have to meet several specifications. The most important aspects are the number channels and the lifetime of the relays. Other factors, such as channel to channel isolation, the contact potential, resistance and maximum voltage is not the limiting factor.

The reason is, that in this case, the voltage is low, there is no ac component involved and the the typical input impedance of high-end multimeters is far more than 100 GΩ [3, 25, 30, 35].

In this work the Keithley (now Tektronix) `Model 2002` was chosen for three reasons. It is a very compact system requiring only a half-sized 2U rack in comparison to the other DMMs, that are typically full-sized 2U rack devices. The other two advantages are the integrated scanner card slot, that allows to to fit a 10 channel scanner card and finally the 20 V range. The latter is interesting for testing the final voltage reference boards, as these have a 15 V output, which is too much for the 10 V range of most DMMs, so that testing the voltage reference Printed circuit boards (PCBs) one would have to switch to the 100 V range and forgo an extra digit of resolution and add more noise.

The test setup consists of a mounting PCB, that holds up to 20 Zener diode. It provides power regulation and a minimal circuit required to support each diode. This circuit is given here:

The compensation network is required when using the ADR1399, because of its very low dynamic impedance as recommended in the data sheet [31]. It is not strictly required for the LM399, but fitted nonetheless, because there are no downsides to it. This makes the board compatible with both types of references. Each Zener output is protected using an output buffer, which provides isolation and short circuit protection. Finally there is a common mode filter at the output to suppress high frequency noise via ground loops.

The two key metrics of concern, that need to measured are popcorn noise and drift.

digital multimeter and a scanner card

Pin	Function	Cable Colour	Pin	Function	Cable Colour
a1, b1	+6 V–+20 V	brown	6	GND	green/white
a2, b2	PD cathode	red	7	LD Cathode	blue/white
a3, b3	LD case (GND)	red/white	8	LD Anode	blue
a4	PD anode (GND)	red/white	9	LD current	green
a5	−6 V–−20 V	brown/white			

As a sidenote, for the pure entertainment of the author, several batches of LM399 Zener diodes were purchased from non-authorized dealers. Some were marked as refurbished, the

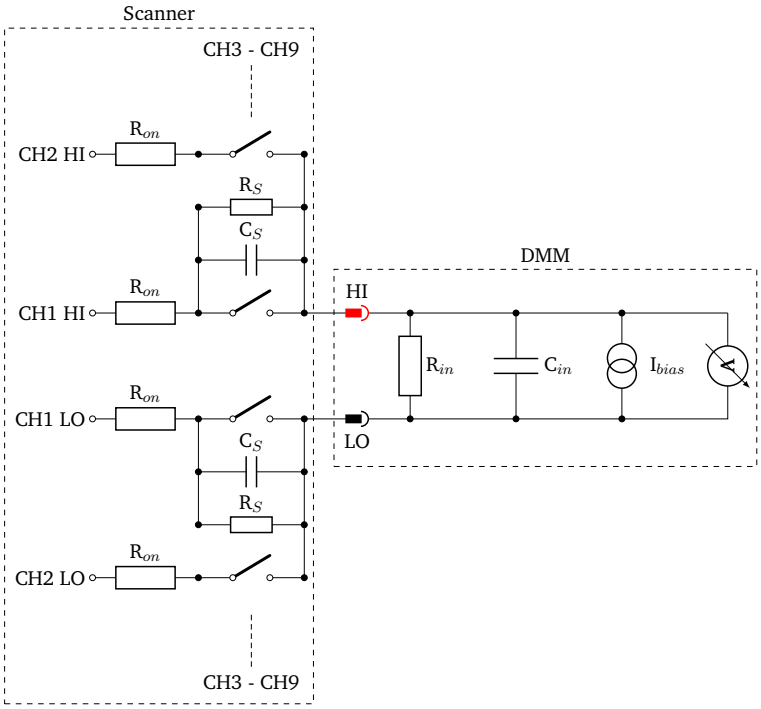

Figure 2.6.: Simplified schematic of the scanner front-end with parasitic elements

others were not marked as such, but clearly were. These so-called refurbished diodes are not to be used in production devices. To entertain and warn the reader a small selection of examples are shown here in figure 2.9. All but one diode, which is shown for comparison, are refurbished.

As it can be clearly seen, the sellers have gone to some effort to hide the fact, that these diodes have been used before. When a through-hole is soldered to the PCB, its legs will be trimmed to match the PCB thickness. In order to conceal this, the legs need to be extended to their original length. The legs of the LM399 are Kovar, because the LM399 is hermetically sealed with a glass seal and Kovar has the same coefficient of expansion as borosilicate glass. The forgers typically weld steel legs to the Kovar legs and then either gold-plate or tin them, as can be seen in fig. 2.10.

Much to the delight of the author the refurbished diodes prove valuable for educational purposes. As the origin and method of extraction from the original circuit is unknown, but can be imagined to be rather savage, the diodes are typically faulty. They can therefore be used to validate the test setup and demonstrate the popcorn noise found in the LM399. A very good example in shown in fig. 2.11.

TODO: Chinese/Ebay Zeners. Welded legs. Photots. Decap one of those.

2.2. Lab Temperature Control

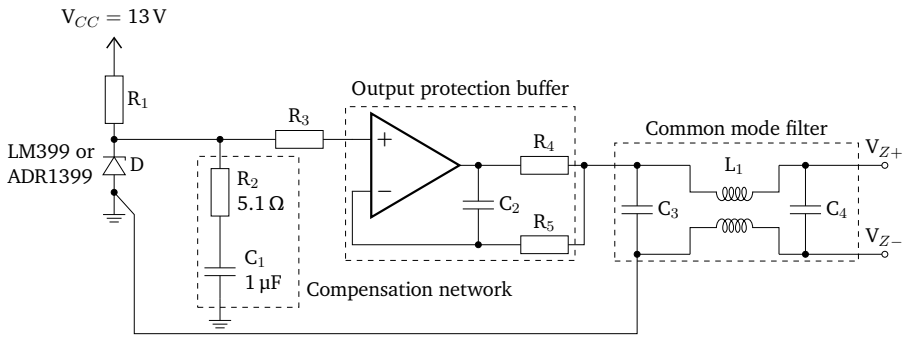

Figure 2.7.: Circuit used for burning in the Zener diodes

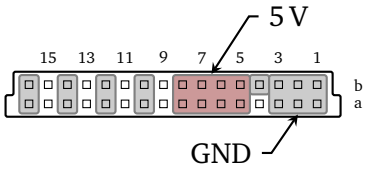

Figure 2.8.: The extension connector used in several Keithley multimeters

Figure 2.9.: Refurbished LM399 Zener diodes. From left to right:

Figure 2.10.: Fake steel legs of a refurbished LM399.

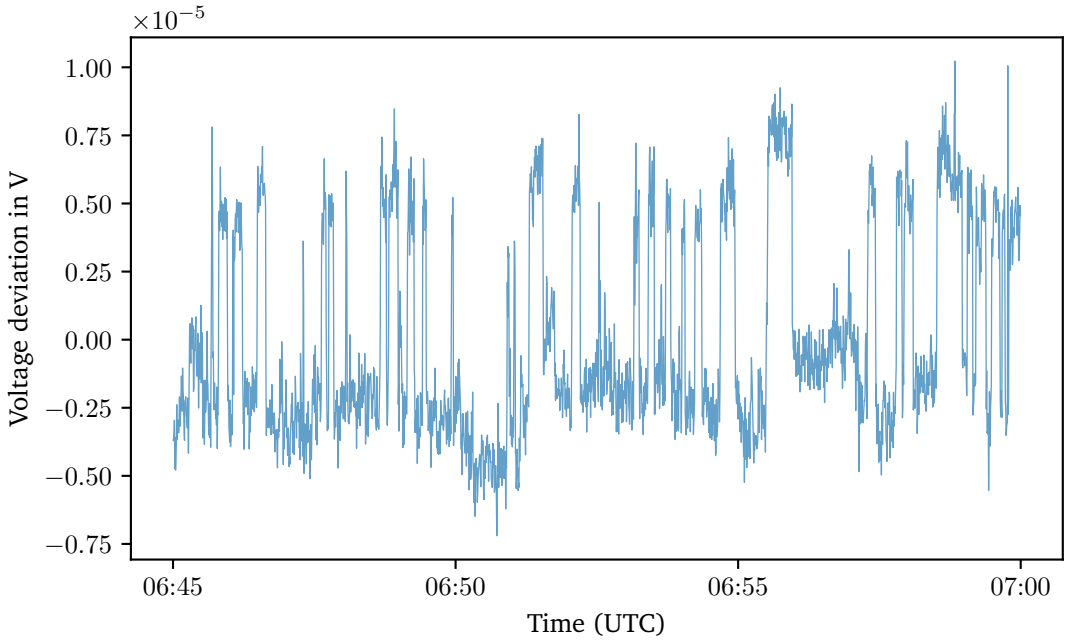

Figure 2.11.: Popcorn noise of a refurbished LM399 (#15) over a period of 15 min.

3. Outlook

Bibliography

[1] *5440B/AF Direct Voltage Calibrator - Service Manual*. John Fluke Mfg. Co. Inc. Dec. 1986.

[2] *8100 Series - 8104 Extended Specifications*. 1.1. Transmille Ltd.

[3] *8588A Reference Multimeter - Product Specifications*. rev. G. Fluke Corporation. Aug. 2022.

[4] D.W. Allan. "Statistics of atomic frequency standards". In: *Proceedings of the IEEE* 54.2 (1966), pp. 221–230. DOI: 10.1109/PROC.1966.4634.

[5] David W. Allan. "Should the classical variance be used as a basic measure in standards metrology?" In: *IEEE Transactions on Instrumentation and Measurement* IM-36.2 (1987), pp. 646–654. DOI: 10.1109/TIM.1987.6312761.

[6] K.J. Åström and R.M. Murray. *Feedback Systems: An Introduction for Scientists and Engineers*. Princeton University Press, 2010. ISBN: 9781400828739. URL: https://fbswiki.org/wiki/index.php/Feedback_Systems:_An_Introduction_for_Scientists_and_Engineers.

[7] James A. Barnes et al. "Characterization of Frequency Stability". In: *IEEE Transactions on Instrumentation and Measurement* IM-20.2 (1971), pp. 105–120. DOI: 10.1109/TIM.1971.5570702.

[8] Patrick Baus. *TinkerforgeAsync*. Version 1.2.0. July 2021. URL: %7Bhttps://github.com/PatrickBaus/TinkerforgeAsync%7D.

[9] K.B. Cook and A.J. Brodersen. "Physical origins of burst noise in transistors". In: *Solid-State Electronics* 14.12 (1971), pp. 1237–1242. ISSN: 0038-1101. DOI: 10.1016/0038-1101(71)90112-2. URL: https://www.sciencedirect.com/science/article/pii/0038110171901122.

[10] Samuel T. Dawkins, John J. McFerran, and Andre N. Luiten. "Considerations on the measurement of the stability of oscillators with frequency counters". In: *IEEE Transactions on Ultrasonics, Ferroelectrics, and Frequency Control* 54.5 (2007), pp. 918–925. DOI: 10.1109/TUFFC.2007.337.

[11] *Digital Multimeters - 34460A, 34461A, 34465A (6½ digit), 34470A (7½ digit)*. Keysight Technologies. June 2022.

[12] Nathan Flowers-Jacobs et al. *The NIST Johnson noise thermometry system for the determination of the Boltzmann constant*. en. Dec. 2017. DOI: 10.6028/jres.122.046. URL: https://tsapps.nist.gov/publication/get_pdf.cfm?pub_id=923576.

[13] C.A. Greenhall. "Spectral ambiguity of Allan variance". In: *IEEE Transactions on Instrumentation and Measurement* 47.3 (1998), pp. 623–627. DOI: 10.1109/19.744312.

[14] Charles Greenhall. "Removal of drift from frequency stability measurements". In: *Telecommunications and Data Acquisition Progress Report* (Nov. 1981).

[15] Paul Horowitz and Winfield Hill. *The Art of Electronics*. 3rd ed. Cambridge: Cambridge University Press, 2015, p. 1224.

[16] David Howe. “Interpreting Oscillatory Frequency Stability Plots”. en. In: 2002 IEEE Intl. Freq. Cont. Symp , New Orleans, LA, Jan. 2002. URL: https://tsapps.nist.gov/publication/get_pdf.cfm?pub_id=105279.

[17] N.J. Kasdin and T. Walter. “Discrete simulation of power law noise (for oscillator stability evaluation)”. In: *Proceedings of the 1992 IEEE Frequency Control Symposium*. 1992, pp. 274–283. DOI: 10.1109/FREQ.1992.270003.

[18] Richard Kaußler. *Richi´s Lab - Linear Technology LM399*. 2021. URL: https://www.richis-lab.de/REF02.htm (visited on 09/02/2022).

[19] Arthur Kay. *Analysis and Measurement of Intrinsic Noise in Op Amp Circuits, Part VIII: Popcorn Noise*. Technote VIII. Texas Instruments Incorporated, Feb. 2008.

[20] Arthur Kay. *Operational Amplifier Noise: Techniques and Tips for Analyzing and Reducing Noise*. Elsevier Science, 2012. ISBN: 9780080942438.

[21] Dan Kegel. *The C10K problem*. May 1999. URL: %7Bhttps://web.archive.org/web/19990508164301/http://www.kegel.com/c10k.html%7D.

[22] *Keysight 3458A Multimeter - Calibration Manual*. Keysight Technologies. July 2022.

[23] Rado Lapuh et al. “Fluke 8588A and Keysight 3458A DMM Sampling Performance”. In: (May 2022). DOI: 10.48550/arXiv.2205.11321.

[24] Paul J Leach, Michael Mealling, and Rich Salz. “A Universally Unique IDentifier (UUID) URN Namespace”. In: *RFC* 4122 (2005), pp. 1–32. URL: %7Bhttps://datatracker.ietf.org/doc/html/rfc4122%7D.

[25] Ivan Lenicek, Damir Ilic, and Roman Malaric. “Determination of digital voltmeter input parameters”. In: *2007 IEEE Instrumentation & Measurement Technology Conference IMTC 2007*. 2007, pp. 1–4. DOI: 10.1109/IMTC.2007.379145.

[26] *LM199/LM399, LM199A/LM399A Precision Reference*. C. Analog Devices, Inc. Dec. 2014.

[27] *LTZ1000/LTZ1000A - Ultra Precision Reference*. D. Analog Devices, Inc. Apr. 2012.

[28] Stefan Machlup. “Noise in Semiconductors: Spectrum of a Two-Parameter Random Signal”. In: *Journal of Applied Physics* 25.3 (1954), pp. 341–343. DOI: 10.1063/1.1721637. eprint: https://doi.org/10.1063/1.1721637. URL: https://doi.org/10.1063/1.1721637.

[29] A.S. McCormack and K.R. Godfrey. “Rule-based autotuning based on frequency domain identification”. In: *IEEE Transactions on Control Systems Technology* 6.1 (1998), pp. 43–61. DOI: 10.1109/87.654876.

[30] *Model 2002 - Multimeter Specifications*. M. Keithley Instruments, Inc. Aug. 2022.

[31] *Oven-Compensated, Buried Zener, 7.05 V Voltage Reference*. A. Analog Devices, Inc. Mar. 2022.

[32] David W. Pessen. “A new look at PID-controller tuning”. In: *Journal of dynamic systems, measurement, and control* 116.3 (1994), pp. 553–557.

[33] Jr. Puckett Jason Niles. “An Electrical and Statistical Study of Burst Noise”. PhD thesis. California Institute of Technology, 1971.

[34] Paul Rako. *Voltage reference drift considerations*. Dec. 2010. URL: https://www.edn.com/voltage-reference-drift-considerations (visited on 09/02/2022).

[35] G. Rietveld. "Accurate determination of the input impedance of digital voltmeters". In: *Science, Measurement and Technology, IEE Proceedings* - 151 (Oct. 2004), pp. 381–383. DOI: 10.1049/ip-smt:20040700.

[36] G.J. Silva, A. Datta, and S.P. Bhattacharyya. *PID Controllers for Time-Delay Systems*. Control Engineering. Birkhäuser Boston, 2007. ISBN: 9780817644239. URL: https://link.springer.com/book/10.1007/b138796.

[37] Guillermo J. Silva, Aniruddha Datta, and S.P. Bhattacharyya. "PI stabilization of first-order systems with time delay". In: *Automatica* 37.12 (2001), pp. 2025–2031. ISSN: 0005-1098. DOI: 10.1016/S0005-1098(01)00165-0. URL: https://www.sciencedirect.com/science/article/pii/S0005109801001650.

[38] Sigurd Skogestad. "Simple analytic rules for model reduction and PID controller tuning". In: *Journal of Process Control* 13.4 (2003), pp. 291–309. ISSN: 0959-1524. DOI: 10.1016/S0959-1524(02)00062-8. URL: https://www.sciencedirect.com/science/article/pii/S0959152402000628.

[39] R. Vilanova and A. Visioli, eds. *PID Control in the Third Millennium: Lessons Learned and New Approaches*. Advances in Industrial Control. Springer London, 2012. ISBN: 9781447124245. DOI: 10.1007/978-1-4471-2425-2_5.

[40] Richard Von Mises. *Über Aufteilungs-und Besetzungswahrscheinlichkeiten*. na, 1939.

[41] *VPR221Z (Z-Foil) - Vishay Foil Resistors*. Vishay Precision Group, Inc. Mar. 2010.

[42] Anders E.E. Wallin. *AllanTools*. 2022. URL: https://github.com/aewallin/allantools (visited on 10/17/2022).

[43] Y. Yamamoto. *Fundamentals of Noise Processes*. Cambridge University Press, 2004. Chap. 9. ISBN: 9780521817486. URL: https://www.nii.ac.jp/qis/first-quantum/e/forStudents/lecture/index.html.

[44] J. G. Ziegler and N. B. Nichols. "Optimum Settings for Automatic Controllers". In: *Journal of Dynamic Systems, Measurement, and Control* 115.2B (June 1993), pp. 220–222. ISSN: 0022-0434. DOI: 10.1115/1.2899060. eprint: https://asmedigitalcollection.asme.org/dynamicsystems/article-pdf/115/2B/220/5546571/220_1.pdf. URL: https://doi.org/10.1115/1.2899060.

A. Appendix

A.1. Multimeter Settings for the Comparison Test

All were configured for maximum stability and similar conversion times using the following settings via SCPI. For better readability, all commands are shown unabridged.

HP 3458A

```
PRESET NORM;  # reset the device
TARM HOLD;  # stop readings
BEEP;
OFORMAT ASCII;  # return text
TRIG AUTO;  # trigger when ready
NRDGS 1,AUTO; # take 1 reading
DCV 10;
AZERO ON;  # enable autozero
NDIG 9;
NPLC 100;
FIXEDZ OFF;  # High input impedance
TARM AUTO;  # enable readings
```

Keithley Model 2002

```
*CLS;  # clear events and errors
*RST;  # reset all settings
*OPC?;  # wait until device is reset
:INITiate:CONTinuous OFF;  # disable continuous initiation
:ABORt;  # place K2002 in idle
:SYSTem:AZERo:STATe ON;  # enable autozero
:SYSTem:AZERo:TYPE SYNChronous;  # azero for every reading
:SYSTem:LSYNc:STATe ON;  # line sync
:SENSe:VOLTage:DC:RANGe:UPPer 20;
:SENSe:VOLTage:DC:DIGits 9;
:SENSe:VOLTage:DC:NPLCycles 10;
:SENSe:VOLTage:DC:AVERage:COUNt 4;  # the averaging length
:SENSe:VOLTage:DC:AVERage:TCONtrol REPeat;  # filter type
:SENSe:VOLTage:DC:AVERage:ADVanced:STATe OFF;
:SENSe:VOLTage:DC:AVERage:STATe ON;  # Enable averaging
:FORMat:DATA REAL,64;  # read data as doubles
:FORMat:ELEMents READing;  # only return the reading
:FORMat:EXPonent HPRecision;  # Scientific notation
:INITiate:CONTinuous ON;  # Enable continuous triggering
```

Keysight 34470A

```
:SYSTem:BEEP;
:ABORt;
*RST;
*CLS;
:CONFigure:VOLTage:DC;
:SENSe:VOLTage:RANGe 10;
:SENSe:VOLTage:ZERO:AUTO ON;  # enable autozero
:SENSe:VOLTage:NPLCycles 100;
:SENSe:VOLTage:IMPEdance:AUTO ON;  # High input impendance
:FORMat:DATA ASCii,9;  # return 9 digits ASCII
```

Keithley DMM6500

```
SYSTem:BEEPer 500, 0.2;
ABORt;
*RST;
*CLS;
:SENSe:FUNCtion:ON "VOLTage:DC";
:SENSe:VOLTage:DC:RANGe:UPPer 10;
:SENSe:VOLTage:DC:LINE:SYNC ON;
:SENSe:VOLTage:DC:AVERage:COUNt 9;  # the averaging length
:SENSe:VOLTage:DC:AVERage:TCONtrol REPeat;  # filter type
:SENSe:VOLTage:AZERo:STATe ON;  # enable autozero
:SENSe:VOLTage:DC:NPLCycles 10;
:SENSe:VOLTage:INPutimpedance AUTO;  # High input impedance
:SENSe:VOLTage:DC:AVERage:STATe ON;  # Enable averaging
:FORMat:DATA ASCii;  # read data as double instead of text
:FORMat:ASCii:PRECision 16;  # return 16 digits ASCII
:DISPlay:VOLTage:DC:DIGits 6;  # set the screen to 6 digits
```